Chemical Geology 266 (2009) 10–18

Contents lists available at ScienceDirect

Chemical Geology

journal homepage: www.elsevier.com/locate/chemgeo

Mantle deformation and noble gases: Helium and neon in oceanic mylonites

Mark D. Kurz [a,*], Jessica M. Warren [b], Joshua Curtice [a]

[a] Marine Chemistry and Geochemistry, MS #25, Clark 421, Woods Hole Oceanographic Institution, Woods Hole, MA 02543, United States
[b] Department of Terrestrial Magnetism, Carnegie Institution of Washington, 5241 Broad Branch Road, NW, Washington, DC 20015-1305, 202.478.8475, United States

ARTICLE INFO

Article history:
Received 25 August 2008
Received in revised form 3 December 2008
Accepted 17 December 2008

Keywords:
Noble gases
Helium isotopes
Neon isotopes
Mylonites
Peridotites
Deformation

ABSTRACT

In an effort to constrain the behavior of noble gases during mantle deformation, we present new helium and neon data in mylonites from subaerial St. Peter and St. Paul Archipelago (Mid-Atlantic Ridge) and the submarine Southwest Indian Ridge. Coupled vacuum crushing and melting experiments show that most of the helium and neon within the mylonites is contained in the mineral matrices rather than fluid or melt inclusions: only 5 to 18% of the total helium is released by crushing. The mylonites and ultramylonites have much higher total helium concentrations than expected, based on their small grain size. The St. Paul's Rocks mylonites have helium contents equivalent to gas-rich MORB glasses, ranging from 6×10^{-6} to 3.8×10^{-5} cc STP He/g. The submarine mylonites and ultramylonites have helium contents between 5×10^{-8} and 4.4×10^{-7} cc STP He/g, compared to 6.2×10^{-9} to 3.6×10^{-8} for the protogranular/porphyroclastic peridotites. Although the dataset is small, it suggests a relationship between metamorphic texture and noble gas abundance, and that mylonitization introduces mantle helium into mineral matrices. The mylonites are extremely fine grained, with an average grain size of ~10 μm, so helium residence in grain boundaries is also plausible. St. Paul's Rocks have modal hornblende, extreme geochemical enrichments in incompatible elements, and high temperature alteration phases (e.g., talc) that are rare or absent in the other samples; mineralogy must also play an important role. The $^{3}He/^{4}He$ ratios in the peridotites are primarily mantle derived, based on comparison with MORB data, suggesting that peridotites reflect the source mantle isotopic compositions. Neon isotopes in St. Paul's Rocks are a mixture of air and normal mantle, and fall along the line defined by MORB glasses. The atmospheric neon signal is preferentially released by crushing in vacuum, suggesting it resides within weakly bound sites in cracks and grain boundaries. He/Ne ratios in St. Paul's Rocks vary widely (~20×) with deformation and mineralogy, with the highest He/Ne ratios (and helium concentration) found in the finest grained ultramylonite peridotite. The neon and helium isotopic data show that mantle gases are preserved in fine-grained mylonites at very high concentrations. The most likely mechanism is diffusive trapping within defects at pressure in the mantle. The relationship between texture and helium abundance in peridotites suggests that metamorphism is a potentially important control on noble gas distribution in the mantle and crust.

1. Introduction

Models for the evolution of noble gases in the earth's mantle and atmosphere are dependant on understanding the residence sites of gases in mantle minerals and in the crust, which control their behavior during melting, outgassing, and metamorphism. Noble gases in ground water and fumaroles are widely used as tracers of crustal versus mantle influence, and may be used as earthquake precursors due to gas release during deformation (e.g., Italiano et al., 2004; Fu et al., 2005). In the laboratory, atmospheric contamination is a ubiquitous problem, but the mechanisms and residence sites of atmospheric contamination in mantle-derived samples are poorly understood. There is also considerable debate regarding the residence of noble gases in the mantle, particularly the explanation for unradiogenic helium and neon isotopic signatures found in some ocean island basalts such as Hawaii, Iceland and Galapagos. The "standard model" holds that unradiogenic helium and neon derive from relatively undegassed reservoirs deep in the earth (e.g., Kurz et al., 1982; Allègre et al., 1983). Recent models suggest an alternative explanation, either by the preservation of ancient isotopic signatures in the residue of melting or by enrichment of gases in ancient lithosphere (e.g., Anderson, 1998a,b; Parman et al., 2005). However, the partitioning behavior of noble gases is not well enough known to constrain these models. Parman et al. (2005) showed that significant amounts of helium were released from experimental olivine charges (in solubility experiments) by crushing in vacuo, suggesting that their

* Corresponding author.
E-mail addresses: mkurz@whoi.edu (M.D. Kurz), jwarren@dtm.ciw.edu (J.M. Warren).

0009-2541/$ – see front matter © 2008 Published by Elsevier B.V.
doi:10.1016/j.chemgeo.2008.12.018

experiments may have been influenced by crystal defects. This study focuses on oceanic mylonites to constrain the relationship between deformation, crystal defects and the noble gas budgets of peridotites.

Many noble gas studies have used basalts as the best representatives of bulk mantle isotopic composition, but it is difficult to infer mantle concentrations from basalt data due to the complex effects of melting, shallow fractionation, and degassing. Peridotites provide important insights into mantle geochemistry, but have not been as extensively studied for noble gases, have large concentration variations due to the presence of fluid inclusions, and oceanic samples often have extensive alteration to serpentine or talc. There have been several noble gas studies of continental peridotite xenoliths, which typically have $^{3}He/^{4}He$ lower than MORB and are assumed to represent the subcontinental lithosphere (e.g., Gautheron and Moreira, 2002; Gautheron et al., 2005). There are few noble gas studies of oceanic peridotites (e.g., Kumagai et al., 2003) and we are unaware of any previous noble gas study of mylonites. Mylonites are the fine-grained products of ductile deformation associated with the down-dip extension of faults (Warren and Hirth, 2006). In the oceanic lithosphere, they are found at both fracture zones and ridge axes. Their temperature of deformation is in the range of 600–800 °C (Jaroslow et al., 1996), suggesting formation depths of ~10–25 km, at

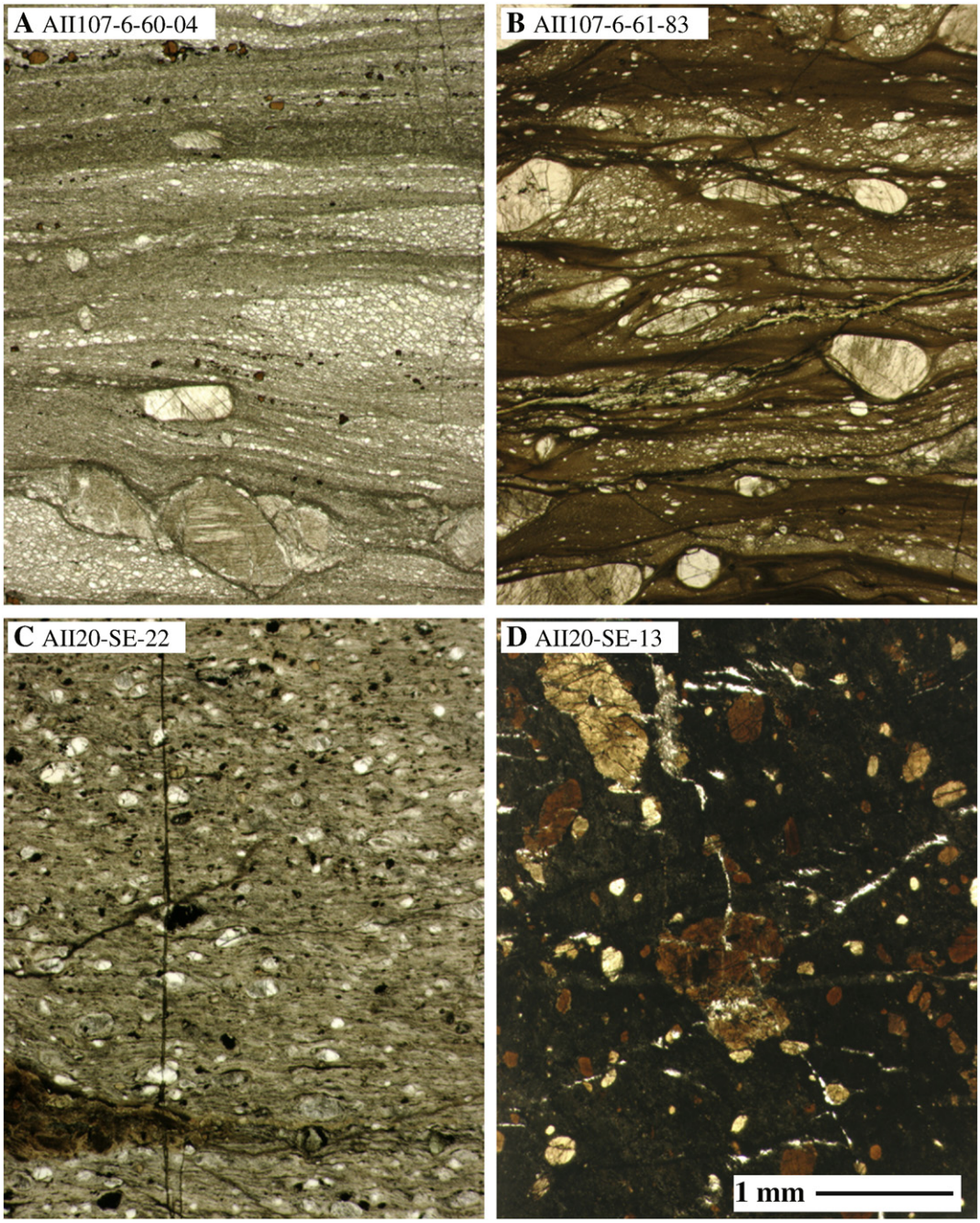

Fig. 1. Photomicrographs of deformed peridotites, all at the same scale; scale bar is shown at the bottom right. (A.) Mylonite AII107-6-60-04 from the Shaka Fracture Zone, illustrating the fine-grained nature of mylonites due to deformation. (B.) Ultramylonite AII107-6-61-83 from the Shaka Fracture Zone. The dark layers contain grains of <10 μm diameter, resulting in multiple grains within the standard 30 μm thin section thickness. (C.) Ultramylonite SE-22 from St. Paul's Rocks. The stretched brown patch at the lower left is hornblende. (D.) Protomylonite SE-13 with a cataclastic overprint from St. Paul's Rocks; brown grains are hornblende. Note that both the St. Paul's samples have a high degree of alteration to talc and magnetite, whereas the Shaka Fracture Zone samples are unaltered.

or below the brittle–ductile transition. One of the most famous localities is exposed at St. Paul's Fracture Zone in the equatorial Atlantic (Darwin, 1845; Melson et al., 1972; Hekinian et al., 2000). The pioneering study of Melson et al. (1972) documented the petrology and geochemistry of the peridotites, with notably high He and Ar concentrations (helium contents were $1–2\times10^{-5}$ cc STP He/g), but did not include isotopic compositions. Staudacher et al. (1989) confirmed high total noble gas concentrations in a single St. Paul's peridotite, with helium isotopic compositions similar to adjacent MORB glasses, but did not discuss the mineralogy or texture of the sample. The new data presented here suggest that mylonites have high noble gas contents, and that deformation *increases* helium concentrations in mantle minerals.

2. Samples and experimental details

The samples were selected from the collection at WHOI, with an emphasis on those with previous textural and geochemical studies. The submarine mylonites primarily come from the Southwest Indian Ridge (SWIR), and were described by Jaroslow et al. (1996) and Warren and Hirth (2006). The protogranular peridotite Circe 97 W from the Central Indian Ridge was described by Engel and Fisher (1975) and Niu (2004). The protomylonitic peridotite PS86-4-36 from the SWIR was selected as it has large serpentinite veins, allowing a separation of the serpentine from the peridotite and preliminary test of the effects of serpentinization on noble gases.

Deformed peridotites are exposed above sea level, at St. Peter and St. Paul Archipelago [Arquipélago de São Pedro e São Paulo, abbreviated here as St. Paul's Rocks, following Darwin (1845)] near the St. Paul fracture zone in the equatorial Atlantic ocean. The samples analyzed here are all mylonites, collected above sea level, and have been previously described for petrology and geochemistry (Frey, 1970; Melson et al., 1972; Thompson 1981; and Roden et al., 1984). They are unusual in mineralogy and trace element geochemistry, particularly in having modal hornblende and light rare-earth element enrichments, which have been used to infer the importance of metasomatism (e.g., Roden et al., 1984) and to distinguish them from other oceanic peridotites (Bonatti, 1990).

Because mylonite grain sizes are so small, typically <100 μm (Fig. 1), it was impossible to make mineral separates, and whole rock chips were used for all the measurements. The samples were gently crushed in stainless steel mortar and pestle, and the 1–3 mm size fraction hand picked using a binocular microscope to avoid saw cuts, visible oxidation, secondary clays, and serpentinization. The chips were sonicated several times in distilled water followed by acetone and air dried in a laminar flow hood. The chips were then placed in an ultra-high-vacuum (UHV) crusher for helium measurements, and crushed 20 to 40 times using a magnetic stainless steel piston and a set of three electromagnets. In order to examine the helium partitioning, the powders were then placed into aluminum foil boats and heated in a single step to 1600 °C using a UHV double vacuum furnace. All the methods for the helium measurements, using a branch tube mass spectrometer locally referred to as MS2, have been previously documented (e.g., Kurz et al., 2004); the helium data are reported in Table 1.

A subset of the samples from St. Paul's Rocks was crushed and melted on a separate extraction line attached to a MAP 215-50 mass spectrometer dedicated to low level neon measurements. Two separate crushing procedures were used on this extraction line, both of which differ from the helium-only procedure. A relatively gentle crushing procedure used the piston action of a modified 3/4″ Varian vacuum valve, while the more vigorous one used manually operated magnetic stainless steel ball bearings, which exert considerably more force, resulting in a finer powder. In both of these cases, the samples were baked to ~120 °C overnight prior to crushing to remove adsorbed atmospheric gases. The powders were then subjected to at least two different heating steps between 600 and 1600 °C. The procedures using this mass spectrometer have been reported by Kurz et al. (2005).

In order to estimate the efficiency of the crushing procedure, 220 mg of ultramylonite AII-107-6-61-83 was crushed in an identical manner to those reported in Table 1, and the grain size distribution was determined using a Beckman Coulter Laser Diffraction Size Analyzer (model LS 13 320 SW). The grain size distribution of the crushed powder is roughly Gaussian with a median grain size of 93 μm, and the relative volume of the various size fractions are: 10%<5.5 μm, 25%<22.9 μm, 50%<93 μm, 75%<241 μm, 90%<406 μm.

Table 1
Helium in oceanic mylonites.

Sample	Lithology	Crush ^{4}He ncc STP/g	Crush ^{3}He/^{4}He (R/Ra)	±	Melt ^{4}He (melt) ncc STP/g	Melt ^{3}He/^{4}He (R/Ra)	±	Total ^{4}He (total) ncc STP/g	Fraction crush
Knipovich Ridge, N. Atlantic									
EN26-26-71	Dunite–mylonite	0.70	2.23	0.37	3.37	2.99	0.11	4.07	0.17
Islas Orcadas Fracture Zone									
IO-11-76-58-30-M	Peridotite–protomylonite	201.0	9.16	0.05					
Shaka Fracture Zone									
A2107-6-61-83*	Peridotite–ultramylonite	51.47	10.28	0.07	392	10.03	0.04	443	0.12
A2107-6-60-4*	Peridotite–mylonite	4.03	10.34	0.14	54.2	10.39	0.05	58.2	0.07
Southwest Indian Ridge									
PS86-4-36	Peridotite–protomylonite	6.94	7.04	0.12	29.43	6.90	0.07	36.37	0.19
PS86-4-36	Serpentine vein	0.711	5.79	0.44	6.15	6.43	0.09	6.86	0.10
Prince Edward Fracture Zone									
PROT5-D19-2	Peridotite–mylonite	7.00	6.13	0.07	46.59	6.68	0.04	53.59	0.13
PROT5-D18-25	Peridotite–ultramylonite	5.54	7.08	0.09	101.0	6.83	0.03	106.5	0.05
Indian Ocean									
CIRCE97-W-OL	Peridotite–protogranular	1.28	6.76	1.29	4.92	6.89	0.28	6.21	0.21
St. Paul's Rocks									
A2-20-SE-13	Horneblend protomylonite	1105	7.08	0.03	4974	6.96	0.02	6079	0.18
A2-20-SE-22	Peridotite ultramylonite	6105	7.04	0.05	32,146	6.95	0.03	38,251	0.16
SE-31	Horneblendite mylonite	537	7.05	0.03	6551	6.95	0.05	7089	0.08
WPli	Horneblend peridotite mylonite	1167	6.86	0.03	20,316	6.89	0.03	21,483	0.05

* Denotes crushed twice.
ncc denotes nano cc.

3. Results and discussion

3.1. Helium contents

The data in Table 1 include results from both crushing and melting experiments, and demonstrate that only a small fraction of the helium in these samples is released by crushing. Among the mylonites, 5 to 17% of the total helium is released by crushing in vacuum, versus 17 to 19% in the protogranular/porphyroclastic peridotites. Crushing is a commonly utilized technique in noble gas geochemistry because a significant fraction of the noble gases in mantle-derived volcanic and ultramafic rocks are often contained within vesicles, melt inclusions and fluid inclusions. The fraction released by crushing is necessarily qualitative, because crushing procedures vary among laboratories, and crushing efficiency can vary with lithology and sample size, as the sample cushions itself. Based on the grain size determination, the results demonstrate that helium does not reside within bubbles or fluid inclusions that are larger than ~93 μm, the median grain size of the crushed powder. Such fluid inclusions are commonly observed in peridotites (Roedder, 1984) but are clearly not an important factor for oceanic mylonites. Crushing alone is therefore not necessarily an appropriate method for noble gas extraction from mylonites.

The samples in Table 1 include a range of deformation conditions. Based on textures observed in thin section, and previous studies of mylonites (Jaroslow et al., 1996; Warren and Hirth, 2006), we use the following categories to define *degree of deformation*: (1) protogranular—no deformation; (2) porphyroclastic—some recrystallization; (3) protomylonite—olivine increasingly recrystallized and pyroxenes stretched and deformed; (4) mylonite—extensive recrystallization of olivine and pyroxenes, down to grain sizes of ~10–100 μm; and (5) ultramylonite—extreme grain size reduction, down to grain sizes <1 μm. Examples of protomylonite, mylonite and ultramylonite textures are shown in Fig. 1. Large porphyroclasts remain in some of the highly deformed rocks, as deformation has been partitioned onto the finest-grained regions of the mylonites (Warren and Hirth, 2006), resulting in an increasingly heterogeneous grain size distribution with decreasing minimum grain size and increasing deformation grade. The combination of the simple deformation classification scheme and the total helium data in Table 1 reveals a relationship between deformation and helium contents, as illustrated in Fig. 2, with the *ultramylonites having the highest helium contents*.

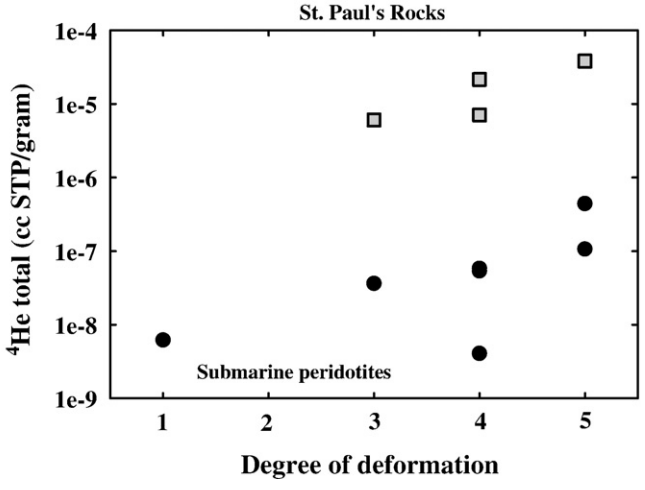

Fig. 2. Relationship between degree of deformation and total ^{4}He contents for the samples in Table 1. The deformation scale is based on examination of thin section deformation textures as follows: 1 = protogranular (no deformation), 2 = porphyroclastic (some recrystallization but no evidence of deformation), 3 = protomylonite (early stages of recrystallization/deformation), 4 = mylonite (extensive recrystallization/deformation), and 5 = ultramylonite (extreme grain size reduction). The St. Paul's Rocks samples (squares) have the highest total helium contents. Within both St. Paul's Rocks and the submarine samples(circles), the ultra-mylonites have the highest total helium contents.

One remarkable aspect of the data in Table 1 and Fig. 2 is the extremely high total helium contents of the samples from St. Paul's Rocks, which range from 6×10^{-6} to 3.8×10^{-5} cc STP He/g. These concentrations are within the typical range for MORB glasses, which are among the highest concentrations measured for mantle-derived materials. The most gas-rich MORB glass sample is a "popping rock" from the mid-Atlantic ridge that has ^{4}He contents of 5.8 to 9.1×10^{-5} cc STP He/g (Staudacher et al., 1989; Moreira et al., 1998). However, MORB glasses are the product of mantle melting. Assuming 10% partial melting and that helium is highly incompatible, a peridotite mantle source for the popping rock would have helium contents of 5.8 to 9.1×10^{-6} cc STP He/g. Therefore, the St. Paul's mylonites have higher helium contents than the most gas rich mantle beneath mid-ocean ridges. The sample with the highest helium concentration (up to 4.6×10^{-5} cc STP/g, see Table 2), SE-22, is an ultramylonite, supporting the relationship between concentration and deformation. However, the presence of hornblende, alteration to talc (Fig. 1), and evidence for melt infiltration (Roden et al., 1984) makes these samples distinct from other peridotites in Table 1. Therefore, the high concentrations in the St. Paul's samples probably relates to both mineralogy and deformation, as discussed further below.

Although the concentrations are dramatically lower in the submarine mylonites, the ^{4}He concentrations in the two oceanic ultramylonites from the SWIR (1.5×10^{-7} to 4.4×10^{-7} cc STP He/g) are higher than the less deformed peridotites, as shown in Fig. 2. There is still a difference of two orders of magnitude in concentration between the submarine ultramylonites and the protogranular sample. Therefore, the relationship between helium content and ductile deformation may exist generally for oceanic mylonites. In the cases where there are several samples from the same region (Shaka and Prince Edward Fracture Zones, St. Paul's Rocks), the most deformed samples always have the highest helium contents.

The single protogranular peridotite (Circe 97 W) has a total helium concentration (6.2×10^{-9} cc STP He/g) which is within the range observed for continental peridotites xenoliths (Gautheron et al., 2005), but significantly lower than any other sample in Table 1. This single sample is not necessarily representative of the mantle, but there are few other peridotite helium measurements with which to compare. Even this least deformed sample has serpentinite veins and secondary minerals. In an effort to determine the influence of serpentinization, relatively pure black serpentine was separated from peridotite sample PS86-4-36. The serpentine/peridotite pair from this sample (Table 1) demonstrates that serpentine has similar isotopic compositions and *lower* ^{4}He contents than the associated peridotite. Therefore, this single serpentine/peridotite pair suggests that serpentinization is not associated with high helium concentrations and that it does not alter mantle ^{3}He/^{4}He.

Even though the measurements were made on fine-grained whole rock samples, it is likely that mineralogy plays a role in helium abundances and that deformation is therefore not the only controlling factor. The highest helium concentrations are observed in the St. Paul's Rocks samples, which are unique due to the presence of hornblende. The lowest total helium concentrations among the mylonites and ultramylonites are observed in the dunite mylonite (EN26-26-71), suggesting that pyroxenes are an important host for helium. Overall, the two extremes in helium concentrations suggest that other mineral phases play an important role. Nevertheless, the relationship between texture and helium abundance in peridotites also shows that deformation has a potentially important control on noble gases in the upper mantle and crust.

3.2. Helium isotopes

The helium isotopic compositions of the peridotite mylonites are mostly within the range of values reported for MORB. Fig. 3 shows the

Table 2
Neon and helium data for St. Paul's Rocks.

Sample	Weight	$^{20}Ne/^{22}Ne$	1 sigma	$^{21}Ne/^{22}Ne$	1 sigma	^{20}Ne (cc STP/g)	$F^{20}Ne$	^{4}He (cc STP/g)	$F^{4}He$	$^{3}He/^{4}He$ (R/Ra)	1 sigma
SE-22*											
Crush-1	0.17959	9.46	0.35	0.0244	0.0033	2.43E−12	0.041	3.02E−08	0.014	9.26	1.01
Crush-2	0.17959	9.93	0.09	0.03325	0.00081	2.56E−11	0.429	7.22E−07	0.340	7.21	0.20
Crush-3	0.17959	10.14	0.08	0.03481	0.00078	3.17E−11	0.531	1.37E−06	0.645	7.16	0.18
Total crush		10.03	0.06	0.03372	0.00056	5.99E−11		2.12E−06		7.21	0.13
Melt											
600 °C	0.16839	10.22	0.06	0.03622	0.00062	5.88E−11	0.118	9.17E−07	0.028	6.95	0.07
1500 °C	0.16839	11.80	0.04	0.05081	0.00059	4.38E−10	0.882	3.23E−05	0.972	6.87	0.07
Total melt		11.62	0.04	0.04908	0.00052	4.97E−10		3.32E−05		6.87	0.07
Total						5.57E−10		3.541E−05			
Fraction crush						0.11		0.06			
SE-22											
5×	0.27809	10.03	0.03	0.03118	0.00028	1.73E−10	0.395	3.65E−06	0.222	6.99	0.13
10×	0.27809	10.20	0.04	0.03290	0.00035	1.04E−10	0.239	3.73E−06	0.227	7.02	0.16
20×	0.27809	10.37	0.04	0.03616	0.00044	9.88E−11	0.226	4.61E−06	0.280	7.13	0.12
40×	0.27809	10.69	0.05	0.03894	0.00059	6.16E−11	0.141	4.45E−06	0.271	6.99	0.17
Total crush		10.24	0.02	0.03381	0.00019	4.38E−10		1.64E−05		7.04	0.07
600 °C	0.17973	10.30	0.05	0.03593	0.00077	7.77E−11	0.169	1.01E−06	0.034	7.33	0.17
800 °C	0.17973	11.30	0.06	0.04711	0.00088	6.05E−11	0.132	1.58E−06	0.053	7.35	0.16
1550 °C	0.17973	11.69	0.03	0.04894	0.00074	2.99E−10	0.651	2.66E−05	0.890	6.95	0.08
1600 °C	0.17973	11.27	0.18	0.04381	0.00213	2.17E−11	0.047	6.99E−07	0.023	6.35	0.07
Total melt		11.38	0.02	0.04625	0.00052	4.59E−10		2.99E−05		6.97	0.07
Total						8.97E−10		4.64E−05			
Fraction crush						0.49		0.35			
WPIi											
1×	0.30028	9.82	0.14	0.03024	0.00063	4.81E−11	0.034	7.99E−08	0.016	7.80	0.27
5×	0.30028	9.98	0.06	0.03165	0.00040	1.20E−10	0.086	6.49E−07	0.129	6.89	0.19
10×	0.30028	10.16	0.04	0.03251	0.00025	1.30E−10	0.092	1.04E−06	0.205	7.23	0.13
20×	0.30028	10.19	0.02	0.03002	0.00014	9.87E−10	0.703	1.35E−06	0.268	7.11	0.10
40×	0.30028	10.41	0.04	0.03605	0.00038	8.45E−11	0.060	1.15E−06	0.229	7.06	0.15
40×	0.30028	10.82	0.07	0.03998	0.00084	3.49E−11	0.025	7.75E−07	0.154	7.00	0.13
Total crush		10.19	0.02	0.03	0.0002	1.40E−09		5.05E−06		7.09	0.06
600 °C	0.19091	10.43	0.04	0.03685	0.00044	8.40E−11	0.127	8.42E−07	0.056	6.91	0.18
1500 °C	0.19091	11.79	0.03	0.05013	0.00054	5.78E−10	0.873	1.41E−05	0.944	6.91	0.11
Total melt		11.62	0.02	0.04844	0.00047	6.62E−10		1.50E−05		6.91	0.10
Total						2.07E−09		2.00E−05			
Fraction crush						0.68		0.25			
SE-13											
1×	0.39828	9.92	0.02	0.02995	0.00028	3.60E−10	0.076	5.93E−08	0.025	7.14	0.46
2×	0.39828	9.97	0.02	0.03049	0.00035	7.79E−10	0.164	2.22E−07	0.094	7.40	0.21
5×	0.39828	9.97	0.02	0.03049	0.00039	9.57E−10	0.202	2.80E−07	0.118	7.01	0.22
10×	0.39828	10.05	0.03	0.03128	0.00018	6.58E−10	0.139	3.03E−07	0.127	7.17	0.20
20×	0.39828	10.15	0.03	0.03179	0.00021	8.14E−10	0.171	5.14E−07	0.216	7.14	0.17
40×	0.39828	10.26	0.01	0.03331	0.00043	6.30E−10	0.133	4.87E−07	0.205	7.36	0.09
40×	0.39828	10.36	0.01	0.03434	0.00048	3.51E−10	0.074	3.13E−07	0.132	7.21	0.18
40×	0.39828	10.46	0.03	0.03550	0.00038	2.00E−10	0.042	1.99E−07	0.084	7.25	0.25
Total crush		10.10	0.01	0.03	0.0001	4.75E−09		2.38E−06		7.22	0.07
600 °C	0.19244	10.07	0.03	0.03275	0.00021	1.59E−09	0.242	2.59E−06	0.711	7.12	0.13
1500 °C	0.19244	11.74	0.02	0.04983	0.00025	4.97E−09	0.758	1.05E−06	0.289	7.13	0.14
Total melt		11.34	0.02	0.04569	0.0002	6.55E−09		3.63E−06		7.12	0.10
Total						1.13E−08		6.01E−06			
Fraction crush						0.42		0.40			
SE-31*											
Crush-1	0.30688	9.81	0.02	0.02897	0.00028	3.05E−10	0.057	3.20E−08	0.049	8.90	0.57
Crush-2	0.30688	9.81	0.02	0.02916	0.00029	1.55E−09	0.291	9.81E−08	0.149	7.19	0.38
Crush-3	0.30688	9.82	0.02	0.02914	0.00018	2.51E−09	0.469	3.29E−07	0.499	6.98	0.14
Crush-4	0.30688	9.81	0.02	0.02951	0.00021	5.06E−10	0.095	9.42E−08	0.143	7.10	0.13
Crush-5	0.30688	9.83	0.02	0.02953	0.00022	4.68E−10	0.088	1.05E−07	0.160	6.99	0.15
Total crush		9.82	0.01	0.02920	0.00012	5.34E−09		6.59E−07		7.12	0.10

* Denotes gentle crushing procedure.

$^{3}He/^{4}He$ for the mylonites from the Southwest Indian Ridge compared to available data for closest MORB glasses. These data suggest that the mylonites dominantly contain mantle helium without contributions from atmospheric or radiogenic helium. Although the data are sparse, the basalts and peridotites from the SWIR Oblique Segment near 14 W have approximately the same $^{3}He/^{4}He$. There are no basalt data from the Islas Orcadas and Shaka Fracture Zones, but the peridotite–mylonite samples from those fracture zones are within the range of basalt glasses from adjacent ridge segments. The Shaka Fracture Zone is apparently a boundary between the high and low $^{3}He/^{4}He$ provinces to the east and west, respectively (Kurz et al., 1998; Georgen et al., 2003; Standish, 2006), and the samples from the fracture zone itself have intermediate $^{3}He/^{4}He$ values of ~10 Ra. The St. Paul's Rocks mylonites also yield $^{3}He/^{4}He$ values that are indistinguishable from adjacent ridge segments (Staudacher et al., 1989; Graham et al., 1992). Thus, peridotite–mylonites provide a new sample type that can potentially be used to characterize geographic mantle isotopic variations, particularly within fracture zones. The combination of the Sr, Nd, and Pb isotopic data of Roden et al. (1984) and the data presented here show that St. Paul's Rocks are within the range of observed values for MORB glasses, but are close to the radiogenic end-member.

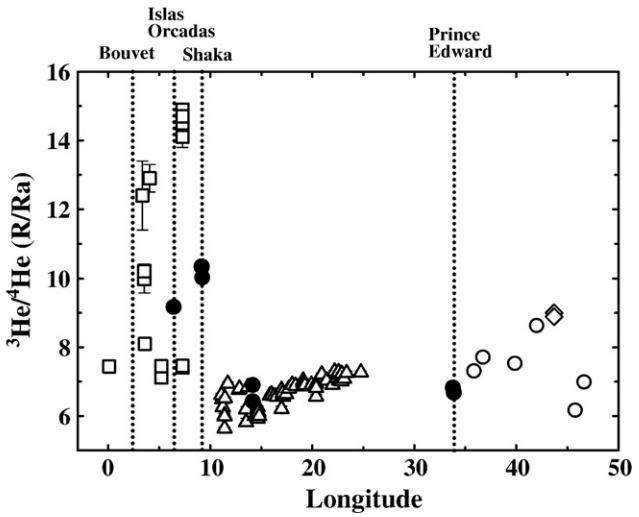

Fig. 3. Helium isotopic data from the mylonite–peridotites (solid circles) as a function of longitude along the Southwest Indian Ridge (Table 1) compared with basalt data from the literature. Data from the literature are all basaltic glasses: Georgen et al. (2003) (triangles); Kurz et al. (1998) (squares); Mahoney et al. (1989) (open circles); Sarda et al. (1988) (diamonds); Standish (2006) (triangles). The dashed lines show the approximate locations of fracture zones relevant to the mylonite–peridotites. The Shaka Fracture Zone defines a boundary between the elevated, but variable, helium isotopic compositions associated with the Bouvet hotspot. The helium isotopic compositions of the mylonites and basalts from the SWIR overlap.

The one sample with ^{3}He/^{4}He outside the range for typical MORB is the dunite mylonite EN26-26-71 (Knipovich Ridge, 2.2 to 3.0 Ra). This sample also is unique among the mylonites in its olivine rich (dunite) mineralogy and low helium concentration. With the exception of this sample, the crushing and melting measurements yielded ^{3}He/^{4}He values that are within experimental error, demonstrating that radiogenic and cosmogenic helium are not important contributors in these samples. The St. Paul's Rocks samples were collected above sea level, and the absence of measurable cosmogenic ^{3}He demonstrates that the exposure ages must be less than ~200 Ka, assuming a sea level cosmogenic ^{3}He production rate of ~116 atoms/g/year.

3.3. Neon isotopes and He/Ne ratios in St. Paul's Rocks

The neon contents and isotopic compositions of the samples from St. Paul's Rocks are given in Table 2. The helium data from these experiments agree with the data presented in Table 1. Total helium contents for samples SE-13 and WPli agree within a few percent; total helium contents for sample SE-22 are more variable, from 3.5 to 4.6×10^{-5} cc STP/g, probably reflecting heterogeneity within the sample itself, which is consistent with the millimeter to centimeter scale heterogeneity observed in thin section (see Fig. 1). The slightly higher fraction of helium in Table 2 released by crushing (up to 40%) relates to differences in the crushing procedure and the greater number of crushing steps in these experiments.

A larger fraction of total neon is released by crushing in vacuo than helium (between 11 and 69%). The neon contents of the St. Paul's Rocks mylonites are extremely high: total ^{20}Ne varies from 5.6×10^{-10} to 1.1×10^{-8} cc STP/g. As a comparison, this is higher than the neon content of the popping rock (8.8×10^{-9} cc STP/g; Moreira et al., 1998). However, the isotopic compositions suggest an important atmospheric component in these samples, and the high neon contents partially relate to atmospheric contamination effects. The fraction of ^{21}Ne* released by crushing varies between 3 and 35%, which is in approximate agreement with the helium results. The neon isotopic data, summarized in Fig. 4, show that these samples fall along the MORB line defined by oceanic basalts (Sarda et al., 1988; Moreira et al., 1998). They therefore contain a mixture of MORB-mantle and air neon. Fig. 4 also illustrates that crushing selectively releases a greater fraction of the atmospheric contamination, with lower ^{20}Ne/^{22}Ne, and that the air neon is therefore trapped in more weakly bound sites in the mylonites. This is also supported by step crushing experiments (e.g., see SE13 in Table 2), which show that the air-like neon is released in the first crushing steps, with progressively higher ^{20}Ne/^{22}Ne released in the later crushing steps. This shows that crushing alone, a common practice in noble gas geochemistry, is not necessarily an appropriate method for peridotite mylonites. The step heating experiments also demonstrate that most of the helium and neon are released at relatively high temperature (>800 °C).

He/Ne ratios provide an important indicator of noble gas fractionation because atmospheric effects can be eliminated; He in oceanic rocks is rarely influenced by atmosphere and Ne abundances can be corrected using the isotopic compositions. Fig. 5 shows a plot of ^{3}He/^{22}Ne extrapolated to solar ^{20}Ne/^{22}Ne to correct for atmospheric contamination [^{3}He/^{22}Ne(ext)], against ^{4}He/^{21}Ne*, where ^{21}Ne* is corrected for atmospheric contamination using ^{21}Ne/^{22}Ne ratios. The mantle production ratio of ^{4}He/^{21}Ne* (from Th and U decay) is relatively constant at $\sim2.2\times10^7$ (Yatsevich and Honda, 1997), so a mantle sample without He/Ne fractionation should have relatively constant values. The correlation between ^{4}He/^{21}Ne* and ^{3}He/^{22}Ne (ext.) in Fig. 5 documents large (~20×) fractionations between helium and neon, most likely post-dating residence in the mantle. Assuming that the production ratio and the popping rock data (Moreira et al., 1998) represent present-day upper mantle values, it is clear that the St. Paul's samples have He/Ne ratios both higher and lower than the mantle.

There is an apparent relationship with deformation, with the highest ^{4}He/^{21}Ne* and ^{3}He/^{22}Ne(ext.) values found in the ultramylonite (SE22) and the lowest values in the coarsest grained protomylonite (SE13, see also Fig. 1). The ultramylonite has the highest ^{4}He abundance but the lowest ^{21}Ne* abundance, so the most deformed sample has the highest ^{4}He while the least deformed (protomylonite) sample has the highest ^{21}Ne*. In addition to being less deformed, the protomylonite (SE13) has more abundant hornblende, so we cannot separate the effects of deformation from mineralogy. If the variations in Fig. 5 are caused by mineralogy alone, they would require that helium and neon have

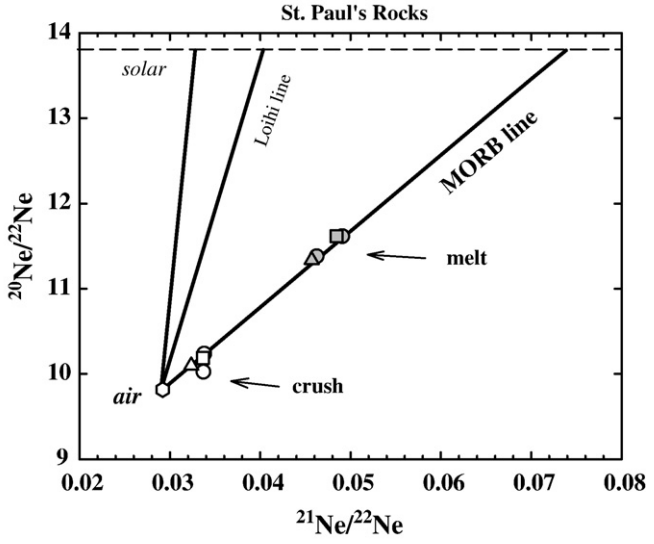

Fig. 4. Neon isotope diagram for St. Paul's Rocks samples (Table 2). For clarity, only the *total* of the crushing and melting experiments is plotted, showing that the neon released by crushing is isotopically closer to air, and thus contains a larger fraction of atmospheric contamination. Hollow symbols indicate crushing measurements, shaded symbols indicate melting of the powder resulting from crushing: triangles (SE-13), squares (WPli), circles (SE-22), and hexagon (SE-31).

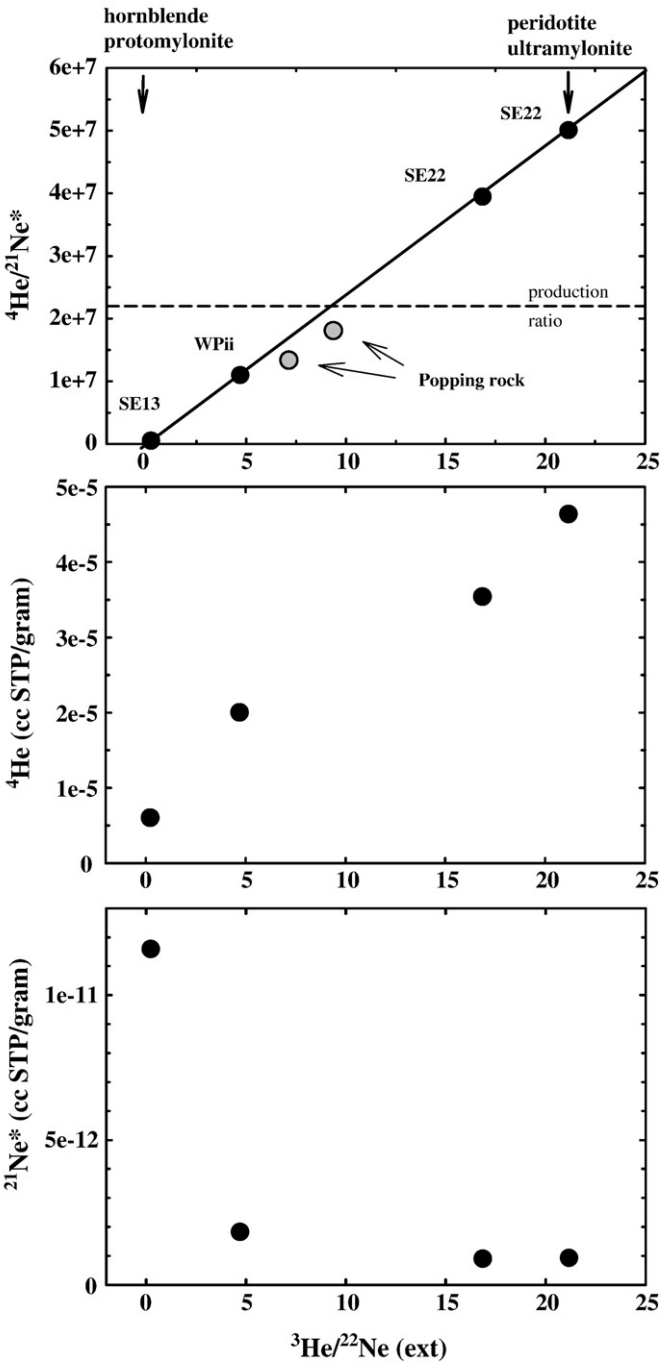

Fig. 5. Comparison of air corrected He/Ne ratios using radiogenic and unradiogenic isotopes, in the samples from St. Paul's Rocks (Table 2). ^{4}He/^{21}Ne* is air corrected using measured ^{4}He and: ^{21}Ne* = ^{22}Ne*(^{21}Ne/^{22}Ne(sample) − ^{21}Ne/^{22}Ne(air). ^{3}He/^{22}Ne (ext) is the ratio extrapolated to a solar ^{20}Ne/^{22}Ne using ^{3}He/^{22}Ne (ext) = ^{3}He/^{22}Ne (measured) * [(^{20}Ne/^{22}Ne(solar) − ^{20}Ne/^{22}Ne(air)) / (^{20}Ne/^{22}Ne(measured) − ^{20}Ne/^{22}Ne(air))]. The four solid circles are the total gas contents from Table 2; popping rock values are from Moreira et al. (1998). Production rate indicated, denoted by dashed line, is the mantle ^{4}He/^{21}Ne production rate as determined by Yatsevich and Honda (1997). The correlation between these two parameters shows that a fractionation between He and Ne occurred after residence in the mantle (see text).

opposite compatibilities in hornblende or some other accessory mineral. An additional complication in this sample suite is the possibility of mantle metasomatism via melt or fluid infiltration, inferred by Roden et al. (1984) to explain the trace element variability. The new data presented here shows that these complex processes, combined with deformation, yields noble gas rich mylonites at St. Paul's Rocks. Unfortunately, noble gas partitioning behaviors in hornblende and the other accessory minerals (Melson et al., 1972) are unknown. The hornblende rich rocks, including SE13, are enriched in incompatible elements and are most likely influenced by melt infiltration/metasomatism, so this is also an important factor. Despite the unconstrained variables, and the small sample set, SE22 is the most deformed peridotite with the simplest mineralogy (spinel peridotite), highest helium contents, and the highest He/Ne ratios. Therefore, we infer that deformation plays a role in the large He/Ne ratio variability, with the highest He/Ne ratios (and total He concentrations) associated with the greatest deformation. Large He/Ne fractionations in oceanic basalts have been extensively discussed in the literature (e.g. Honda and Patterson, 1999), but the physical mechanism(s) for the fractionation have not been identified.

3.4. Noble gas residence sites and origin of the high concentrations

Although there is still considerable uncertainty regarding mantle noble gas partitioning, it is well established that helium and neon are highly incompatible elements in olivine, clinopyroxene, and orthopyroxene (Marty and Lussiez, 1993; Kurz et al., 2004; Parman et al., 2005; Heber et al., 2007). Therefore, we assume that the high helium and neon concentrations are not related to equilibrium partitioning into these minerals. Although the mineralogy of the St. Paul's Rocks samples is more complex, there is a dependence of helium concentrations on deformation in both (St. Paul's Rocks and SWIR) sample suites, with highest helium concentrations in the finest grained peridotites. We consider three possibilities for noble gas storage in these samples: (i) in fluid or melt inclusions, (ii) at crystal defect sites and (iii) on grain boundaries.

The results of the crushing experiments rule out an important role for melt or fluid inclusions for noble gas storage in these samples; crushing releases a small fraction of the mantle gases. This conclusion is consistent with results from the combined helium and neon experiments, though the crushing efficiency varies. In addition, examination of thin sections failed to reveal any fluid or melt inclusions. The experiments, and limitations of optical microscopy, do not exclude the role of small inclusions (<10 μm). However, the step heating experiments on the crushed powders (Table 2) demonstrate that helium and neon are only released at temperatures greater than 800 °C (e.g., see SE22), which also suggests that the noble gases are tightly bound and reside primarily within mineral grains. This argument assumes that fluid inclusions would be released at relatively low temperatures from the powders, which was observed in only one case (helium in SE13). Therefore, the combined crushing and heating experiments suggest that fluid inclusions are not an important residence site for helium and neon in these samples.

During deformation, defects (e.g., dislocations and subgrain boundaries) are continually created. Gradients in dislocation density promote the dynamic recrystallization that leads to grain size reduction in mylonites. At steady state, there is a balance between the creation and removal (by recrystallization and recovery) of defects. The relatively high concentrations of noble gases in mylonites may indicate storage of noble gases at crystal defect sites within recrystallized grains. One problem with this hypothesis is that individual mylonite grains are so small that they may not retain helium. However, the high observed concentrations indicate that mantle helium is retained during post-deformation residence in the mantle, prior to emplacement, and simple diffusion calculations place some constraints on the minimum time scales required. We assume a mean grain size of 50 μm, that mylonites are formed at 700 °C (Jaroslow et al., 1996), and that high temperature helium diffusion measurements in olivine and clinopyroxene can be extrapolated to 700 °C (yielding D values of 4.4×10^{-18} and 2.4×10^{-14} cm^2/s, respectively; Trull and Kurz, 1993). Using an approximation for diffusion time scales ($x=(Dt)^{1/2}$), mantle residence times must be

less than 2000 years for olivine and 0.3 year for clinopyroxene to retain helium in the mylonites. These mantle residence times are too short even to explain the minimum residence time, i.e. transport from the mantle to the crust, because they require mantle upwelling rates orders-of-magnitude faster than known spreading rates. Therefore, if helium resides within defects in olivine and clinopyroxene grains, the diffusion length scale must be much larger than the grain sizes defined by thin section observations (e.g., Fig. 1).

Grain boundaries are another factor that may influence noble gas abundances and transport rates (Hiraga et al., 2004; Baxter et al., 2007; Hiraga et al., 2007). Hiraga et al. (2003) demonstrated that olivine–olivine grain boundaries have a characteristic width of 5 nm. Hiraga et al. (2007) and Baxter et al. (2007) suggest that finer grained rocks can store a larger volume of noble gases at grain interfaces than coarser grained rocks. With decreasing grain size, the volume occupied by grains decreases as a function of r^3 (where r is grain radius), whereas the volume occupied by grain boundaries decreases as a function of r^2. Hence, a rock with a smaller grain size has a larger relative grain boundary volume. Hiraga et al. (2007) estimate that an order of magnitude decrease in grain size results in an order of magnitude increase in the storage capacity of grain interfaces, and that shear zone deformation leads to mantle with enhanced concentrations of incompatible elements. Baxter et al. (2007) used laboratory step heating experiments to study grain boundary partitioning and also concluded that bulk noble gas storage is greater in finer grained rocks. It is generally assumed that grain boundary diffusion is orders-of-magnitude faster than volume diffusion (e.g., Hiraga, 2007; Baxter et al., 2007). Therefore, the mylonite data presented here are consistent with this hypothesis *only* if the grain boundaries are tightly sealed enough to retain helium and neon, as interconnected grain boundaries would result in fast diffusion paths, and loss from the rock. The time scale for grain boundary diffusion is not clear because helium grain boundary diffusion rates are not known, nor are the time scales and geometry of shear zone deformation. If we assume that the mylonites are produced in ~100 m wide shear zones, and reside within the mantle for ~1 Ma, grain boundary diffusion rates would have to be less than 10^{-6} cm^2/s over this length scale.

The observation that the highest He/Ne ratios are found in the most deformed peridotite (at St. Paul's Rocks) provides some constraints on the residence sites. Assuming that typical mantle gases have He/Ne ratios close to the production ratio (see Fig. 5), then the residence site in the most deformed samples must produce a helium enrichment during trapping. This suggests a diffusive mechanism, because helium and neon have similar equilibrium partitioning behavior in olivine and clinopyroxene (e.g., Heber et al., 2007). One possibility is that helium preferentially diffuses into newly created defects during deformation. Using the 1 Ma time scale, and the 700 °C olivine diffusion coefficient, helium could diffuse into defects ~10 μm deep within olivine grains. Neon diffusion coefficients are not known but should be significantly slower than helium due to the larger atomic radius, which could then explain the observed helium enrichments. One might expect the opposite behavior within grain boundaries, with helium escaping faster than neon via fast diffusion paths, leading to a helium deficit in the gas left behind. Therefore, we interpret the He/Ne fractionation as preliminary evidence for helium residence within defects in the mylonites.

As discussed above, St. Paul's Rocks are anomalous due to the aerial exposure of abyssal peridotite, extreme geochemical enrichments, and the abundance of hornblende in the peridotites. Hence, this region could be associated with mantle of anomalous composition, including enrichment in helium. The high helium concentrations at St. Paul's Rocks is probably not related to the presence of hornblende, because the highest helium contents and He/Ne are found in the peridotite mylonite which has the least hornblende (SE22). It is also noteworthy that the dunite from the Knipovich Ridge has extremely low helium concentrations. This may be due to the mineralogy of the sample, which does not contain pyroxene in significant volume (unlike the peridotites). Alternatively, low helium concentrations may be due to the loss of helium to migrating melt, as dunites are generally interpreted as the conduits for melt flow in the mantle (Kelemen et al., 1995).

The high helium concentrations in the peridotite mylonites may also reflect their resistance to weathering, in comparison to undeformed abyssal peridotites. Mylonites are generally <10% altered, whereas most abyssal peridotites are >70% altered, suggesting that mylonites have a smaller number of cracks due to their higher fracture toughness, which is related to smaller grain size (deMartin et al., 2004). As cracks are potential pathways for fast diffusion of noble gases out of peridotites, the high concentrations of noble gases in mylonites may be therefore relate to grain size and crack density. Conversely, the neon isotopic data suggests that atmospheric neon is weakly bound within the mylonites, and is probably introduced along cracks.

4. Conclusions

The new data presented here show that mantle deformation and metamorphism can be an important control on noble gas contents in the crust and upper mantle. The differences in mineralogy among the samples, which range from dunite to spinel peridotite to hornblende mylonite, suggests that deformation is not the only factor and that mineralogy almost certainly plays an important role. However, the highest helium contents are found in the most deformed, finest grained, ultramylonite peridotites. The experiments also show that crushing in vacuum typically releases a small fraction of the mantle noble gases, so crushing is not necessarily the best method for this rock type. Most of the mantle helium and neon is released by heating of the crushed powders only at high temperatures (>800 °C) which implies that it must be tightly bound within the minerals. The high helium concentrations in the ultramylonites, coupled with the high He/Ne within the St. Paul's Rocks ultramylonite, suggest that the noble gases are trapped within defects in the mineral grains, implying that deformation takes place in a gas-rich mantle environment.

Since deformation in the mantle and crust takes place along active faults, these data provide an explanation for the observation that gas release may be associated with earthquakes. They also provide a new possible explanation for the existence of primordial noble gases deep within the earth. If deformation took place in the early earth, such mylonitized mantle could potentially retain high gas contents and preserve unradiogenic isotopic compositions. As documented here, the mylonites do not release helium and neon until relatively high temperatures, and could potentially survive the subduction process. Although the present data set is small, it provides the first evidence that deformation can influence noble gas abundances in the upper mantle.

Acknowledgments

We gratefully acknowledge valuable discussions with H. Dick, P. Kelemen, and G. Hirth in selecting the samples and interpreting the results, and the assistance of D. Lott with the instrumentation. We thank R. Sorrell and J. Donnelly for assistance with the grain size determination, and S. Hart and J. Blusztajn for providing the Circe and St. Paul's Rock samples. We particularly wish to thank Manuel Moreira and Junji Yamamoto for their insightful comments regarding He/Ne ratios, and Pete Burnard for his helpful review. This work was partially supported by funds from the National Science Foundation OCE07-27044 and OCE05-25864 and a WHOI Independent Study Award. We thank the organizers of the ICGG for their hard work and patience.

References

Allègre, C.J., Staudacher, T., Sarda, P., Kurz, M., 1983. Constraints on evolution of Earth's mantle from rare gas systematics. Nature 303, 762–766.

Anderson, D.L., 1998a. The helium paradoxes. Proc. Natl. Acad. Sci. U. S. A. 95, 4822–4827.

Anderson, D.L., 1998b. A model to explain the various paradoxes associated with mantle noble gas geochemistry. Proc. Natl. Acad. Sci. 95, 9087–9092.
Baxter, E.F., Asimow, P.D., Farley, K.A., 2007. Grain boundary partitioning of Ar and He. Geochim. Cosmochim. Acta 71, 434–451.
Bonatti, E., 1990. Subcontinental mantle exposed in the Atlantic Ocean on St Peter-Paul islets. Nature 345, 800–802.
Darwin, C., (1845) Journal of researches into the natural history and geology of the countries during the voyage of the H.M.S. Beagle round the world. 2nd edition, London.
deMartin, B.J., Hirth, G., Evans, B., 2004. Experimental constraints on thermal cracking of peridotite at oceanic spreading centers. AGU Geophys. Monogr. 148, 167–185.
Engel, C.G., Fisher, R.L., 1975. Granitic to ultramafic rock complexes of the Indian Ocean ridge system, western Indian Ocean. Geol. Soc. Amer. Bull. 86, 1553–1578.
Frey, F.A., 1970. Rare earth and potassium abundances in St. Paul's Rocks. Earth Planet. Sci. Lett. 7, 351–360.
Fu, C.C., C.H., Yang, T.F., V., Walia , Chen, 2005. Reconnaissance of soil gas composition over the buried fault and fracture zone in Southern Taiwan. Geochem. J. 39, 427–439.
Gautheron, C., Moreira, M., 2002. Helium signature of the subcontinental mantle. Earth Planet. Sci. Lett. 199, 39–47.
Gautheron, C., Moreira, M., Allegre, C., 2005. He, Ne, and Ar composition of the European lithospheric mantle. Chem. Geol. 217, 97–112.
Georgen, J.E., Kurz, M.D., Dick, H.J.B., Lin, J., 2003. Low $^{3}He/^{4}He$ ratios in basalt glasses from the western Southwest Indian Ridge (10°–24°E). Earth Planet. Sci. Lett. 206 (3–4), 509–528.
Graham, D.W., Jenkins, W.J., Schilling, J.G., Thompson, G., Kurz, M.D., Humphris, S.E., 1992. Helium isotope geochemistry of mid-ocean ridge basalts from the South Atlantic. Earth Planet. Sci. Lett. 110, 133–147.
Heber, V.S., Brooker, R.A., Kelley, S.P., Woods, B.J., 2007. Crystal-melt partitioning of noble gases for olivine and clinopyroxene. Geochim. Cosmochim. Acta 71, 1041–1061.
Hekinian, R., Juteau, T., Gracia, E., Sichler, B., Sichel, S., Udintsev, G., Apprioual, R., Ligi, M., 2000. Submersible observations of Equatorial Atlantic mantle: the St. Paul fracture zone region. Mar. Geophys. Res. 21, 529–560.
Hiraga, T., Anderson, I.M., Kohlstedt, D.L., 2003. Chemistry of grain boundaries in mantle rocks. Am. Mineral. 88, 1015–1019.
Hiraga, T., Anderson, I.M., Kohlstedt, D.L., 2004. Grain boundaries as reservoirs of incompatible elements in the Earth's mantle. Nature 427, 699–703.
Hiraga, T., Hirschmann, M.M., Kohlstedt, D.L., 2007. Equilibrium interface segregation in the diopside–forsterite system II: applications of interface enrichment to mantle geochemistry. Geochim. Cosmochim. Acta 71, 1281–1289.
Honda, M., Patterson, D.B., 1999. Systematic elemental fractionation of mantle-derived helium, neon, and argon in mid-oceanic ridge glasses. Geochim. Cosmochim. Acta 63, 2863–2874.
Italiano, F., Martinelli, G., Rizzo, A., 2004. Geochemical evidence of seismogenic-induced anomalies in the dissolved gases of thermal waters: a case study of Umbria (Central Apennines, Italy) both during and after the 1997–1998 seismic swarm. Geochem. Geophys. Geosystems 5 Article Number: Q11001.
Jaroslow, G.E., Hirth, G., Dick, H.J.B., 1996. Abyssal peridotite mylonites: implications for grain size sensitive flow and strain localization in oceanic lithosphere. Tectonophysics 245, 17–37.
Kelemen, P.B., Shimizu, N., Salters, V.J.M., 1995. Extraction of mid-ocean-ridge basalt from the upwelling mantle by focused flow of melt in dunite channels. Nature 375, 747–753.
Kumagai, H., Dick, H.J.B., Kaneoka, I., 2003. Noble gas signatures of abyssal gabbros and peridotites at an Indian Ocean core complex. Geochem. Geophys. Geosyst. 4 (12), 9107. doi:10.1029/2003GC000540.
Kurz, M.D., Jenkins, W.J., Hart, S.R., 1982. Helium isotopic systematics of oceanic islands: implications for mantle heterogeneity. Nature 297, 43–47.
Kurz, M.D., le Roex, A., Dick, H., 1998. Isotope geochemistry of the mantle beneath the Bouvet Triple Junction. Geochim. Cosmochim. Acta 62, 841–852.
Kurz, M.D., Curtice, J., Lott, D.E., Solow, A., 2004. Rapid helium isotopic variability in Mauna Kea shield lavas from the Hawaiian Scientific Drilling Project. Geochem. Geophys. Geosystems 5, Q04G14. doi:10.1029/2002GC000439.
Kurz, M.D., Moreira, M., Curtice, J., Lott, D., Mahoney, J., Sinton, J., 2005. The neon isotope anomaly in the mantle beneath the superfast spreading East Pacific rise. Earth Planet. Sci. Lett. 232, 125–142.
Mahoney, J.J., Natland, J.H., White, W.M., Poreda, R., Bloomer, S.H., Fisher, R.L., Baxter, A.N., 1989. Isotopic and geochemical provinces of the western Indian Ocean spreading centers. J. Geophys. Res. 94, 4033–4052.
Marty, B., Lussiez, P., 1993. Constraints on rare gas partition coefficients from analysis of olivine-glass from a picritic mid-ocean ridge basalt. Chem. Geol. 106, 1–7.
Melson, W.G., Hart, S.R., Thompson, G., 1972. St. Paul's Rocks, Equatorial Atlantic: petrogenesis, radiometric ages, and implications on sea floor spreading. Geol. Soc. Amer. Mem. 132, 241–271.
Moreira, M., Kunz, J., Allegre, C., 1998. Rare gas systematics in popping rock: isotopic and elemental compositions in the upper mantle. Science 279, 1178–1181.
Niu, Y., 2004. Bulk rock major and trace element compositions of abyssal peridotites: implications for mantle melting, melt extraction, and post-melting processes beneath mid-ocean ridges. J. Petrol. 45, 2423–2458.
Parman, S., Kurz, M.D., Hart, S.R., Grove, T.L., 2005. Helium solubility in olivine and its implication for high $^{3}He/^{4}He$ in ocean island basalts. Nature 437, 1140–1143.
Roden, M.K., Hart, S.R., Frey, F.A., Melson, W.G., 1984. Sr, Nd, and Pb isotopic and REE geochemistry of St. Paul's Rocks: the metamorphic and metasomatic development of an alkali basalt mantle source. Contrib. Mineral. Petrol. 85, 376–390.
Roedder, E., 1984. Fluid Inclusions, Reviews of Mineralogy, Volume 12. Mineralogical Society of America.
Sarda, P., Staudacher, T., Allègre, C.J., 1988. Neon isotopes in submarine basalts. Earth. Planet. Sci. Lett. 91, 73–88.
Standish, J.J., (2006) The influence of ridge geometry at the ultraslow-spreading Southwest Indian Ridge (9°–25°E): basalt composition sensitivity to variations in source and process. PhD Thesis, MIT/WHOI Joint Program, 286pp.
Staudacher, T., Sarda, P., Richardson, S.H., Allegre, C.J., Sagna, I., Dmitriev, L.V., 1989. Noble gases in basalt glasses from a Mid-Atlantic Ridge topographic high at 14 N: geodynamic consequences. Earth. Planet. Sci. Lett. 96, 119–133.
Thompson, G., 1981. St. Peter and St. Paul's Rocks and the surrounding sea floor. Technical Report WHOI-81-98. Woods Hole Oceanographic Institution.
Trull, T., Kurz, M.D., 1993. Diffusivity of ^{3}He and ^{4}He in olivine and clinopyroxene at magmatic and mantle temperatures. Geochim. Cosmochim. Acta 57, 1313–1324.
Warren, J.M., Hirth, G., 2006. Grain size sensitive deformation mechanisms in naturally deformed peridotites. Earth. Planet. Sci. Lett. 248, 438–450.
Yatsevich, I., Honda, M., 1997. Production of nucleogenic neon in the Earth from natural radioactive decay. J. Geophys. Res. 102, 10291–10298.